Oersted Initial Field Model

As a secondary payload poised atop a Delta rocket, the Danish geomagnetic research satellite Oersted was launched February 23, 1999 from Vandenberg AFB in California. The principle aim of the Oersted mission is to accurately map Earth's global magnetic field, a field which has changed significantly in the twenty years since NASA's enormously successful Magsat mission. After attaining a near polar orbit with altitudes ranging from 638 to 849 km, the mini-sat class Oersted spacecraft extended an 8 meter long gossamer mast carrying both vector and scalar magnetometers. These instruments measure both the direction and strength of the ambient magnetic field. The orientation of the measured field relative to the fixed stars is determined using an effectively non-magnetic Star Imager bonded to the vector magnetometer. The Oersted Initial Field Model is derived from both scalar and calibrated, oriented vector magnetic data using the time-tested technique of spherical harmonic analysis. The thousands of measured data fitted by this main field model were carefully selected to reduce contributions from electric currents flowing in Earth's partially ionized upper atmosphere and from magnetic storms caused by the fluctuating solar wind. Moreover, the weighted least squares fit to these select data reflects the anisotropic residual covariance needed to account for small errors in the observations, notably in the angle of rotation about the bore-sight of the single Star Imager. As expected, the model fits the measured field to about one part in ten thousand. Although the Oersted Initial Field Model includes Gauss coefficients through degree and order 19, we only recommend use of coefficients from this initial field model up to degree 14 at most.

Ørsted Initial Field Model

N. Olsen[1], R. Holme[2], G. Hulot[3], T. Sabaka[4], T. Neubert[5], L. Tøffner-Clausen[5],
F. Primdahl[1,6], J. Jørgensen[6], J.-M. Léger[7], D. Barraclough[8], J. Bloxham[9],
J. Cain[10], C. Constable[11], V. Golovkov[12], A. Jackson[13], P. Kotzé[14], B. Langlais[3],
S. Macmillan[8], M. Mandea[3], J. Merayo[6], L. Newitt[15], M. Purucker[4], T. Risbo[16],
M. Stampe[1], A. Thomson[8], C. Voorhies[4]

Abstract. Magnetic measurements taken by the Ørsted satellite during geomagnetic quiet conditions around January 1, 2000 have been used to derive a spherical harmonic model of the Earth's magnetic field for epoch 2000.0. The maximum degree and order of the model is 19 for internal, and 2 for external, source fields; however, coefficients above degree 14 may not be robust. Such detailed models exist for only one previous epoch, 1980. Achieved rms misfit is 2 nT for the scalar intensity and 4 nT for the vector components perpendicular to the magnetic field. This model is of higher detail than the IGRF 2000, which for scientific purposes related to the Ørsted mission it supersedes.

Introduction

Twenty years after the Magsat mission, the Ørsted satellite was launched on February 23, 1999 in a near polar orbit with an inclination of 96.5°, a perigee at 638 km and an apogee at 849 km. The principal aim of the Ørsted mission [*Neubert et al.*, in preparation] is to accurately map the Earth's magnetic field.

The goal of this paper is to present an accurate "snapshot" of the geomagnetic field at epoch 2000.0 based on geomagnetic quiet days around January 1, 2000. To reduce contamination of the lower degree expansion coefficients by spatial aliasing, the analysis was performed through degree and order 19 for the internal field and 2 for the external field. However, we only recommend use of coefficients up to degree 14 at most.

Ørsted data from May to September 1999 were used to derive the IGRF 2000 [*Olsen and Sabaka*, 2000]. How-

[1] Danish Space Research Institute, Copenhagen, Denmark
[2] GeoForschungsZentrum, Potsdam, Germany
[3] IPGP, Paris, France
[4] NASA/GSFC, Greenbelt/MD, USA
[5] Danish Meteorological Institute, Copenhagen, Denmark
[6] Institute for Automation, DTU, Lyngby, Denmark
[7] CEA-Direction des Technologies Avancées, France
[8] British Geological Survey, Edinburgh, UK
[9] Harvard University, Cambridge MA, USA
[10] Florida State University, Tallahassee, FL, USA
[11] University of California, San Diego, CA, USA
[12] IZMIRAN, Troitsk, Russia
[13] University of Leeds, UK
[14] Hermanus Magnetic Observatory, S. Africa
[15] Natural Resources Canada
[16] Copenhagen University, Denmark

ever, the satellite was still in the commissioning phase before September 1999, and the measurements used for the present study are more accurate.

Data selection and pre-processing

Data from geomagnetic quiet conditions between December 18, 1999 and January 21, 2000 were selected according to the following criteria: $Kp \leq 1+$ for the time of observation, $Kp \leq 2o$ for the previous three hour interval, $|Dst| < 10$ nT and $|d(Dst)/dt| < 3$ nT/hr. To reduce contributions from ionospheric currents at middle and low latitudes, only night-side data (local time about 22:00) were selected. Vector data were used for dipole latitudes $|\lambda_{\text{dip}}| < 50°$, and scalar data for $|\lambda_{\text{dip}}| \geq 50°$ or if attitude data were not available. To further reduce contributions from polar cap ionospheric currents, only data for which the dawn-dusk interplanetary magnetic field component was weak ($|B_y| < 3$ nT) were used. An equal area distribution was approximated by decimating the data to measurement times at least $30s/\sin\theta$ apart, where θ is geocentric co-latitude. All orbits were visually inspected and those suspected of contamination by external currents were removed. Attitude information over the South Atlantic Anomaly (SAA) was sparse due to radiation effects on the star imager, resulting in a paucity of vector data there. Since this region is close to the dip-equator (the thin line in Figure 1) where vector data are mandatory to avoid the Backus effect [*Stern and Bredekamp*, 1975], 66 data points during four orbits on the geomagnetic quiet days October 9 and November 26, 1999 were added to constrain field direction in this region. Figure 1 shows the distribution of the 2148 scalar data points and 3957 vector

Figure 1. Data distribution. Scalar measurements are shown by small and vector measurements by larger symbols. Open circles present additional vector data to fill the gap in the SAA.

triplets used for the model.

The attitude accuracy of the Ørsted star imager (SIM) is anisotropic: determination of the SIM bore-sight direction ("pointing") is more accurate than determination of the rotation around the bore-sight ("rotation"). This results in relatively more noise in the rotation angle, which is also more sensitive to distorting effects like instrument blinding (for instance by the moon). This attitude anisotropy results in correlated errors between the magnetic components, which should be taken into account when deriving field models [*Holme and Bloxham*, 1996; *Holme*, 2000].

Let $\hat{n}$ be the unit vector of the SIM bore-sight, and let **B** be the observed magnetic field vector. **B** and $\hat{n}$ define a new coordinate system (provided they are not parallel), and the magnetic residual vector $\delta\mathbf{B} = (\delta B_B, \delta B_\perp, \delta B_3)$ can be transformed such that the first component, δB_B, is in the direction of **B**, the second component, $\delta B_\perp$, is aligned with $(\hat{n} \times \mathbf{B})$, and the third component, δB_3, is aligned with $\mathbf{B} \times (\hat{n} \times \mathbf{B})$. The last two components are perpendicular to the magnetic field. In this coordinate system, the errors on the different field components are uncorrelated.

Let ψ be the attitude error of the bore-sight (pointing error), χ that around bore-sight (rotation error) and let σ be the (attitude independent) error of the scalar intensity. Considering only linear terms in ψ and χ, the component δB_B is independent of attitude errors. δB_3 is affected only by pointing errors, whereas $\delta B_\perp$ is influenced by both pointing errors and rotation errors [*Holme*, 2000]. Since the rotation uncertainty is believed to be the main error source, the component $B_\perp$ is more contaminated than the two other components and should be down-weighted.

As an example, Figure 2 shows the residuals of the nightside part of orbit # 4343. The upper panels present residuals $(\delta B_r, \delta B_\theta, \delta B_\phi)$ as a function of colatitude θ; the lower panels present the residuals as $(\delta B_B, \delta B_\perp, \delta B_3)$. The noise is clearly spread over all three components in the
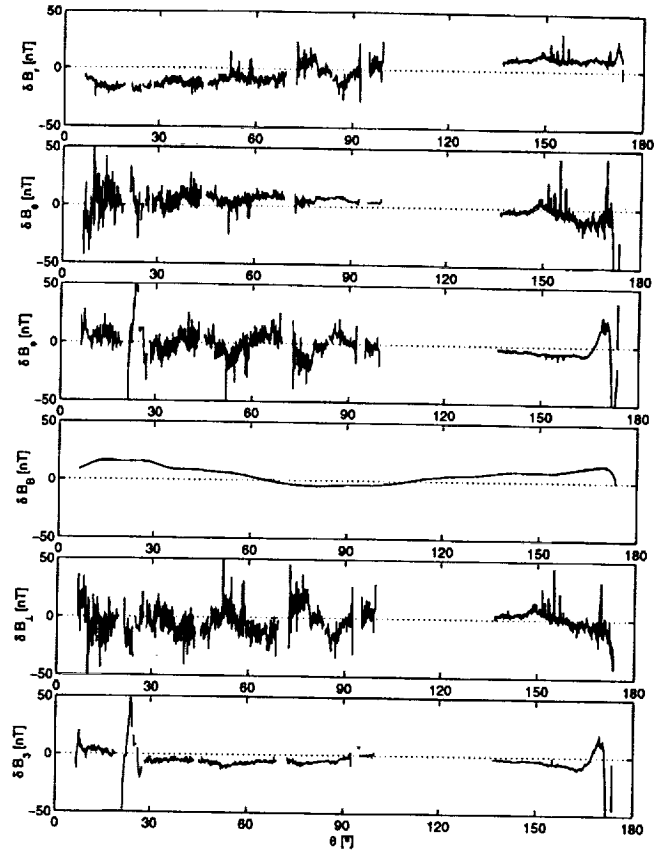
Figure 2. Residuals (observations minus values predicted by the model of Table 2) as a function of co-latitude θ for the nightside part of orbit # 4343, December 22, 1999, 01:21 – 02:11 UT. $Kp = 0o$ and $Dst = +9\,nT$.

$(\delta B_r, \delta B_\theta, \delta B_\phi)$ system, but is concentrated in $\delta B_\perp$ in the $(\delta B_B, \delta B_\perp, \delta B_3)$ system. δB_3 remains slightly more noisy than δB_B due to pointing uncertainty and field-aligned currents. In particular, δB_3 signatures at $\theta \approx 25°$ and 170° are caused by auroral field-aligned currents. The gap in the vector components between $\theta = 100°$ and 135° is due to moon-blinding of the star imager.

Most all data selected span 35 days during which the field changes by up to 20 nT due to secular variation (SV). It has been decided to account for this change by propagating all observations to epoch 2000.0 since this a) reduces the model misfit of δB_B and δB_3 by 10% and 6%, respectively (that of $\delta B_\perp$ is not changed); and b) reduces the magnetic power R_n for all degrees above $n = 12$ (mean reduction: 17%). The latter indicates that SV between neighboring measurements taken at different epochs will, if not corrected for, produce spurious high degree signals. Two different SV models were used: an updated version of the IGRF 2000 SV model [*Macmillan and Quinn*, 2000] and a model generated from Ørsted data spanning over 9 months. Negligible difference

was found, so it was decided to use the Ørsted SV model for internal consistency. This model is still in development, and will be the subject of a future publication.

Model parameterization and estimation

The magnetic field $\mathbf{B} = -\mathrm{grad}\, V$ can be derived from a magnetic scalar potential V which is expanded into terms of spherical harmonics:

$$V = a \left\{ \sum_{n=1}^{19} \sum_{m=0}^{n} \left(g_n^m \cos m\phi + h_n^m \sin m\phi \right) \left(\frac{a}{r} \right)^{n+1} P_n^m(\cos\theta) \right.$$

$$+ \sum_{n=1}^{2} \sum_{m=0}^{n} \left(q_n^m \cos m\phi + s_n^m \sin m\phi \right) \left(\frac{r}{a} \right)^{n} P_n^m(\cos\theta)$$

$$+ Dst \cdot \left[\left(\frac{r}{a} \right) + Q_1 \left(\frac{a}{r} \right)^2 \right] \cdot$$

$$\left. \left[\tilde{q}_1^0 P_1^0(\cos\theta) + \left(\tilde{q}_1^1 \cos\phi + \tilde{s}_1^1 \sin\phi \right) P_1^1(\cos\theta) \right] \right\}.$$

$a = 6371.2$ km is the mean radius of the Earth, (r, θ, ϕ) are geocentric coordinates, $P_n^m(\cos\theta)$ are the associated Schmidt-normalized Legendre functions and (g_n^m, h_n^m) and (q_n^m, s_n^m) are the Gauss coefficients describing internal and external source fields, respectively. The coefficients $\tilde{q}_1^0, \tilde{q}_1^1$ and $\tilde{s}_1^1$ account for the Dst-dependent part of the external dipole. Its internal, induced, counterpart is represented via the factor $Q_1 = 0.27$, a value found from Magsat data by *Langel and Estes* [1985]. The model has 410 parameters (399 static internal, 8 static external, and 3 coefficients of Dst-dependency).

The coefficients are estimated by an iterative least-squares fit, minimizing $\mathbf{e}^T \mathbf{C}_d^{-1} \mathbf{e}$ where the residuals $\mathbf{e} = \mathbf{d}_{\mathrm{obs}} - \mathbf{d}_{\mathrm{mod}}$ are the differences between observations and values predicted by the model, and $\mathbf{C}_d$ is the *a-priori* covariance of residuals due to data errors and fields left unmodeled. To account for the anisotropic attitude accuracy, $\mathbf{C}_d$ was assigned the form of Eq. 18 of *Holme and Bloxham* [1996], with $\sigma = 2.25$ nT, $\psi = 10''$ and $\chi = 60''$ (these values are justified by the *a-posteriori* model misfit, pre-flight instrument error estimates are $3''$ and $20''$ for SIM and 0.2 nT for the vector magnetometer).

When solving the least-squares problem, three iterations were found to be sufficient. Outliers were removed after the second iteration; as outlier selection criterion we have used 15 nT for δB_B and δB_3 but 30 nT for $\delta B_\perp$. If one of the component residuals was above its threshold value, all three components were removed.

Results and Discussion

Number of data points fitted, residual means and rms misfits of the model are given in Table 1. The anisotropy of rms misfit in $(\delta B_B, \delta B_\perp, \delta B_3)$ components is much larger than

	N_{tot}	N_{out}	mean	rms
$\delta F_{\mathrm{polar}}$	1322	13	-0.16	2.77
$\delta F_{\mathrm{non-polar}} + \delta B_B$	4783	49	0.04	1.87
$\delta B_\perp$	3957	49	1.12	8.38
δB_3	3957	49	-0.04	2.62
δB_r	3957	49	0.63	4.79
δB_θ	3957	49	-0.20	5.58
δB_ϕ	3957	49	-0.36	5.21

Table 1. Number N_{tot} of data points, number N_{out} of removed outliers, means, and rms misfits (in nT) for the different components. "Polar" denotes data with $|\lambda_{\mathrm{dip}}| > 50°$.

in spherical components. Figure 3 shows the data residuals as a function of dipole co-latitude. The largest residuals in δB_B are found in the southern polar cap ($\theta_{\mathrm{dip}} > 170°$) and are attributed to ionospheric currents in the summer polar cap. Electrical conductivity is smaller in the northern (winter) polar cap ionosphere due to absence of solar irradiation, and therefore the δB_B residuals in the northern polar cap ($\theta_{\mathrm{dip}} < 10°$) exhibit a smaller scatter than their counterparts in the southern polar cap. However, contributions from ionospheric polar electrojets are present even in the northern auroral zone ($\theta_{\mathrm{dip}} \approx 23°$).

The large rms and mean values for $\delta B_\perp$ (present even when the data are weighted isotropically) confirm the necessity to downweight this component using the covariance matrix $\mathbf{C}_d$. A resolution analysis shows that $B_\perp$ resolves only 6% of the model parameters if the data are treated in this way, but 24% if data errors are assumed to be isotropic. The corresponding values for B_B (B_3) are 38% (27%) and 27% (23%), whereas the resolving power of F is 30% and 27%, respectively. The model fits the data with a (normalized) chi-squared misfit of 1.01 which is close to unity, consistent with
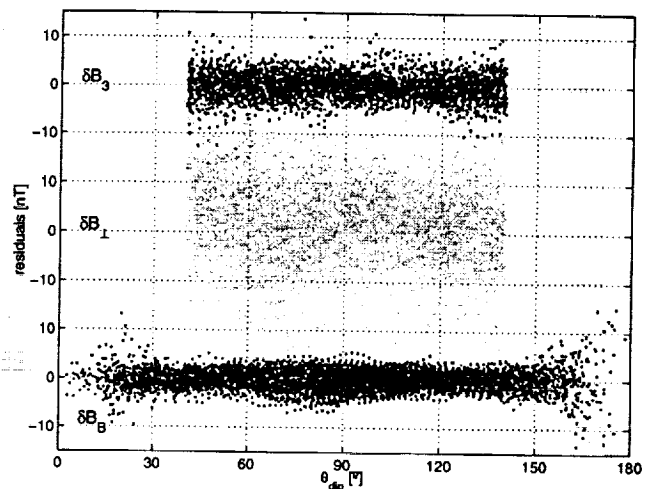
Figure 3. Residuals as a function of dipole co-latitude.

the weighting (*a-priori* data errors σ, ψ, χ) being correct. The model coefficients are given in Table 2. Only internal coefficients up to $n = 14$ are listed; the complete model is available at www.dsri.dk/Oersted/Field_models/OIFM/.

Experiments with various truncation levels of the spherical harmonic expansion gave the largest changes in the southern polar cap ($\theta_{dip} > 175°$), centered around the magnetic pole. This indicates that contributions from ionospheric current systems in the summer hemisphere are probably present in the data and model in spite of our attempt to minimize external current contributions by careful data selection according to geomagnetic indices and IMF B_y.

To address these contributions will likely require inclusion of more satellite data, ground data, and perhaps co-estimation of ionospheric field parameters. Doing so is beyond the scope of our model.

The model presented here provides a firm basis for studies of the ionospheric, magnetospheric, lithospheric and core fields. The initial model from Ørsted, the first magnetic mapping mission of the "International Decade of Geopotential Research", will also aid interpretation of the additional, continuous, high precision measurements of Earth's time-varying geomagnetic and gravitational fields acquired by forthcoming missions like Champ and SAC-C.

References

Holme, R., Modelling of attitude error in vector magnetic data: application to Ørsted data, *Earth, Planets and Space, submitted*, 2000.

Holme, R., and J. Bloxham, The treatment of attitude errors in satellite geomagnetic data, *Phys. Earth Planet. Int.*, **98**, 221–233, 1996.

Langel, R. A., and R. H. Estes, Large-scale, Near-Earth magnetic fields from external sources and the corresponding induced internal field, *J. Geophys. Res.*, **90**, 2487–2494, 1985.

Macmillan, S., and J. M. Quinn, The 2000 revision of the joint UK/US geomagnetic field models and an IGRF 2000 candidate model, *Earth, Planets and Space, submitted*, 2000.

Olsen, N., and T. J. Sabaka, Determination of the IGRF 2000 model, *Earth, Planets and Space, submitted*, 2000.

Stern, D. P., and J. H. Bredekamp, Error enhancement in geomagnetic models derived from scalar data, *J. Geophys. Res.*, **80**, 1776–1782, 1975.

N. Olsen, Danish Space Research Institute, Juliane Maries Vej 30, DK – 2100 Copenhagen Ø, Denmark. (e-mail: nio@dsri.dk)

Internal coefficients (g_n^m, h_n^m):

n	m	g_n^m	h_n^m
1	0	-29617.37	
1	1	-1729.24	5185.65
2	0	-2268.46	
2	1	3068.92	-2481.77
2	2	1670.76	-457.62
3	0	1340.16	
3	1	-2288.34	-227.87
3	2	1252.09	293.28
3	3	714.08	-491.32
4	0	932.11	
4	1	786.66	273.21
4	2	249.82	-231.70
4	3	-403.30	119.53
4	4	111.25	-303.65
5	0	-217.06	
5	1	351.98	42.76
5	2	222.06	171.19
5	3	-130.52	-132.88
5	4	-168.40	-39.42
5	5	-12.92	106.44
6	0	71.40	
6	1	67.40	-16.86
6	2	74.17	64.34
6	3	-160.81	65.34
6	4	-5.77	-61.03
6	5	17.00	0.80
6	6	-90.38	43.96
7	0	79.07	
7	1	-73.59	-65.03
7	2	-0.04	-24.69
7	3	33.10	6.17
7	4	9.11	24.03
7	5	7.03	14.87
7	6	7.08	-25.34
7	7	-1.31	-5.71
8	0	23.92	
8	1	5.99	12.18
8	2	-9.20	-21.05
8	3	-7.74	8.63
8	4	-16.54	-21.39
8	5	8.95	15.30
8	6	7.03	8.76
8	7	-7.97	-14.92
8	8	-7.01	-2.46
9	0	5.30	
9	1	9.63	-19.91
9	2	2.93	13.07
9	3	-8.58	12.50
9	4	6.32	-6.23
9	5	-8.76	-8.31
9	6	-1.53	8.46
9	7	9.13	3.88
9	8	-4.24	-8.29
9	9	-8.09	4.88
10	0	-3.03	
10	1	-6.46	1.87
10	2	1.56	0.34
10	3	-2.95	4.12
10	4	-0.32	4.94
10	5	3.67	-5.86
10	6	1.11	-1.18
10	7	2.09	-2.84
10	8	4.41	0.24
10	9	0.42	-1.98
10	10	-0.94	-7.67
11	0	2.54	
11	1	-1.58	0.36
11	2	-1.83	1.29
11	3	1.47	-0.85
11	4	-0.08	-2.59
11	5	0.18	0.90
11	6	-0.74	-0.65
11	7	0.78	-2.82
11	8	1.85	-0.89
11	9	0.01	-1.08
11	10	1.05	-1.98
11	11	4.07	-0.44
12	0	-2.53	
12	1	-0.51	-0.40
12	2	0.19	0.25
12	3	0.86	2.38
12	4	-0.22	-2.66
12	5	0.85	0.54
12	6	-0.60	0.29
12	7	0.30	0.02
12	8	-0.34	-0.03
12	9	-0.50	0.21
12	10	-0.26	-1.00
12	11	-0.16	-0.48
12	12	0.30	0.54
13	0	-0.24	
13	1	-0.81	-0.81
13	2	0.44	0.23
13	3	0.07	1.79
13	4	-0.39	-0.49
13	5	1.31	-0.95
13	6	-0.46	-0.03
13	7	0.74	0.63
13	8	-0.30	0.21
13	9	0.32	0.62
13	10	-0.14	0.29
13	11	0.26	-0.23
13	12	0.24	-0.24
13	13	-0.08	-1.03
14	0	-0.57	
14	1	-0.06	0.12
14	2	-0.20	-0.74
14	3	-0.13	0.19
14	4	-0.18	0.40
14	5	0.18	-0.11
14	6	-0.06	0.42
14	7	0.05	0.20
14	8	0.26	0.26
14	9	0.03	0.30
14	10	0.59	0.03
14	11	-0.41	-0.03
14	12	0.04	0.05
14	13	0.38	0.04
14	14	0.44	0.21

External coefficients:

n	m	q_n^m	s_n^m
1	0	22.43	
1	1	0.84	-3.73
2	0	1.57	
2	1	0.29	-0.32
2	2	-0.52	-0.04

n	m	$\tilde{q}_n^m$	$\tilde{s}_n^m$
1	0	-0.59	
1	1	0.04	0.10

Table 2. Expansion coefficients of internal (g_n^m, h_n^m) and external (q_n^m, s_n^m) contributions, in nT. $\tilde{q}_n^m$ and $\tilde{s}_n^m$ present the Dst-dependent part of the external coefficients.